Calculation of Available Transfer Capability Using Hybrid Chaotic Selfish Herd Optimizer and 24 Hours RES-thermal Scheduling

Kingsuk Majumdar[1*], *Provas Kumar Roy*[2] *and Subrata Banerjee*[3]

(1. Department of Electrical Engineering, Dr. B C Roy Engineering College, Durgapur 713206, India;
2. Department of Electrical Engineering, Kalyani Government Engineering College, Kalyani 741235, India;
3. Department of Electrical Engineering, NIT Durgapur, Durgapur 713209, India)

Abstract: As fossil fuel stocks are being depleted, alternative sources of energy must be explored. Consequently, traditional thermal power plants must coexist with renewable resources, such as wind, solar, and hydro units, and all-day planning and operation techniques are necessary to safeguard nature while meeting the current demand. The fundamental components of contemporary power systems are the simultaneous decrease in generation costs and increase in the available transfer capacity (ATC) of current systems. Thermal units are linked to sources of renewable energy such as hydro, wind, and solar power, and are set up to run for 24 h. By contrast, new research reports that various chaotic maps are merged with various existing optimization methodologies to obtain better results than those without the inclusion of chaos. Chaos seems to increase the performance and convergence properties of existing optimization approaches. In this study, selfish animal tendencies, mathematically represented as selfish herd optimizers, were hybridized with chaotic phenomena and used to improve ATC and/or reduce generation costs, creating a multi-objective optimization problem. To evaluate the performance of the proposed hybridized optimization technique, an optimal power flow-based ATC was enforced under various hydro-thermal-solar-wind conditions, that is, the renewable energy source-thermal scheduling concept, on IEEE 9-bus, IEEE 39-bus, and Indian Northern Region Power Grid 246-bus test systems. The findings show that the proposed technique outperforms existing well-established optimization strategies.

Keywords: Available transfer capability (ATC), biogeography-based optimization (BBO), chaotic map, chaotic selfish herd optimizer (CSHO), grey wolf optimizer (GWO), optimum power flow (OPF), power generation cost (PGC), renewable energy sources (RES), selfish herd optimizer (SHO)

1 Introduction

According to the North American Electric Reliability Council (NERC), the definition of “available transfer capability” (ATC) is the amount of additional power that can be moved over the lines that are already in place without infringing on the power systems’ limits. The hourly and daily ATC data must be openly accessible as per the guidelines of the Federal Energy Regulatory Commission (FERC). Presently, the complexity of power systems is very high because the modern frameworks and distributed generators (DGs) are connected to the grid.

The system operator must provide ATC in an open-access, publicly assessable domain on an hourly and daily basis [1]. According to the World Bank and Central Electricity Authority (CEA) India [2-3], the world’s power demand is increasing rapidly. Constructing a new transmission line for highly populated countries such as India and China is almost impossible. An ATC assessment provides appropriate information to ensure that these types of power transactions continue to take place over the current transmission lines without infringing on the limits of the power system [1, 4-5].

Therefore, the real-time calculation of ATC always adds an extra burden to the optimization process. The benefit of real-time ATC assessment is that assessment occurs during the actual operation of power networks

Manuscript received January 14, 2023; revised June 13, 2023; accepted August 23, 2023. Date of publication December 31, 2023; date of current version September 1, 2023.
* Corresponding Author, E-mail: kingsuk.majumdar5@gmail.com
Digital Object Identifier: 10.23919/CJEE.2023.000032

when power transactions are happening. An operator can have ten times more power transaction conditions in the existing network if the ATC is known in advance. Scheduling renewable energy sources (RESs) with thermal generation units introduces additional uncertainties that require careful consideration. This problem cannot be ignored from a financial engineering perspective [1]. In the present era, power system networks involve grids, DGs, RESs, and flexible AC transmission systems (FACTS), which make power-flow equations much more complex and nonlinear [6]. Hence, known linearization methods cannot accurately evaluate the ATC. Several computational techniques have been used to obtain an accurate ATC by maintaining the voltage stability, thermal limit, reactive power generation limit, and other power system constraints within limits; the techniques are listed below.

(1) Using an optimal power flow (OPF) method [7].

(2) Using a distributed contingency analysis method [8].

(3) Using a conceding voltage stability monitoring process [9-10].

(4) Using a distributed state estimations process [11-12].

(5) Using a distributed control for distribution power networks [13-14].

Some standard optimization techniques, such as biogeography-based optimization (BBO), grey wolf optimization (GWO), and selfish herd optimizer (SHO), are widely used to evaluate the OPF. Hence, these optimization tools can also be used for ATC calculations. Therefore, a real-time ATC can be determined by modeling a multiarea OPF problem that considers both the equality and inequality criteria. Time and memory complexities are no longer major issues for modern computers. Meta-heuristic algorithms are a class of computational techniques employed to obtain near-optimal solutions to optimization problems. Genetic algorithms are well suited for addressing combinatorial optimization problems because of their ability to efficiently identify a solution of satisfactory quality within a reasonable time frame. Meta-heuristic algorithms are a potent set of procedures that aim to optimize one or more objective functions for a particular problem while considering the constraints and limitations. The techniques in question are problem agnostic, meaning that they do not rely on any particular characteristics of the problem at hand and are thus applicable to a broad spectrum of problems. Metaheuristic algorithms possess numerous advantages over nonmetaheuristic techniques. These advantages include the capacity to discover approximate solutions to optimization problems, wide-ranging applicability, and the ability to generate nearly optimal solutions in a computationally efficient manner. Furthermore, the computation of ATC using the OPF method involves intricate nonconvex and nonlinear methodologies. Therefore, the classical techniques are considered inadequate. Hence, the use of metaheuristics is required. Therefore, the ATC can be evaluated in real time using OPF by applying metaheuristic techniques. Briefly, the main arguments of this study are as follows.

(1) SHO and chaotic selfish herd optimizer (CSHO) algorithms are employed to formulate the multiarea ATC problem using OPF.

(2) Usually the generation cost is not considered when computing the ATC. However, in this study, a multi-objective optimization problem that includes generation costs is considered [15-17].

(3) According to the ATC calculation, the integration of hydro-wind-solar units with thermal power plants aims to reduce the expenses incurred in the production of active power and safeguard the environment.

(4) The problem formulation presented in this article considers the scheduling of thermal, hydro, wind, and solar energy systems, along with the fluctuation in energy demand over a 24-h period and enhancement of the ATC during this time frame [18-21].

The remainder of this paper is organized as follows. Section 2 presents a clear mathematical representation of the proposed problem, including relevant information on wind, solar, thermal, and hydroelectric resources. In Section 3, we describe the implementation of the proposed hybrid chaotic selfish herd optimizer and selfish herd optimizer algorithms in detail. Section 4 presents the investigation on the use of the aforementioned method under different test conditions, namely the IEEE 9-bus, IEEE 39-bus, and Indian Northern Regional Power Grid (NRPG) 246-bus systems. Finally, we conclude the paper and

discuss future implications in Section 5.

2 System modelling using mathematics

The mathematical foundations for wind, solar, hydrothermal, and ATC calculations are applied individually in this section.

2.1 Generation of wind energy and its cost

The generation of wind power is unpredictable [22-24]. The probability density function in Eq. (1) can be used to forecast wind speed, as shown below [25]

$$pdw(S_h, S_f, vl) = \exp\left(-\left(\frac{vl}{S_f}\right)^{S_h}\right)\frac{S_h}{S_f}\left(\frac{vl}{S_f}\right)^{S_h-1} \quad (1)$$

The cumulative density function (CDF) for wind speed is denoted by Eq. (2)

$$cdw(S_h, S_f, vl) = 1 - \exp\left(-\left(\frac{vl}{S_f}\right)^{S_h}\right) \quad (2)$$

A linear model can be used to illustrate the relationship between wind speed and viability of wind power generation, as shown in Eq. (3)

$$wnd = \begin{cases} wnd_R & vl \leqslant vl \leqslant vl_{out} \\ 0 & vl < vl_{in} \text{ or } vl \geqslant vl_{out} \\ \dfrac{wnd\left(vl - vl_{in}\right)}{vl_R - vl_{in}} & vl_{in} \leqslant vl \leqslant vl_{out} \end{cases} \quad (3)$$

The authors computed the likelihood of wind power under wind and zero wind conditions using Eqs. (4) and (5) as follows

$$P_{wnd}(wnd = 0) = cdw(vl_{in}) - (cdw(vl_{out}) - 1) = 1 + \exp\left(-\left(\frac{vl_{out}}{S_f}\right)^{S_h}\right) - \exp\left(-\left(\frac{vl_{in}}{S_f}\right)^{S_h}\right) \quad (4)$$

$$P_{wnd}(wnd = wnd_R) = cdw(vl_{out}) - (cdw(vl_R) - 1) = \exp\left(-\left(\frac{vl_{out}}{S_f}\right)^{S_h}\right) - \exp\left(-\left(\frac{vl_{in}}{S_f}\right)^{S_h}\right) \quad (5)$$

where *cdw* is a random variable (*wnd*) obtained using Eqs. (4) and (5) that can be rewritten as follows

$$f_{wnd}(wnd) = \begin{cases} 1 & wnd > wnd_R \\ 0 & wnd < 0 \\ \dfrac{vl_{in} S_h H_{wnd}}{wnd_R S_f}\left(\dfrac{\left(wnd_R + H_{wnd}\right)vl_{in}}{wnd_R S_f}\right)\times \\ \exp\left(-\dfrac{\left(wnd_R + H_{wnd}\right)vl_{in}}{wnd_R S_f}\right) \\ 0 < wnd \leqslant wnd_R \end{cases} \quad (6)$$

where

$$H_{wnd} = -1 + \left(\frac{vl_R}{vl_{in}}\right) \quad (7)$$

Wind power output is not constant because of variations in wind speed. Consequently, the amount of wind power produced is sometimes less than the demand (an overstated scenario), whereas at other times, it is greater than the load demand (under the estimated scenario). Both scenarios include two additional cost factors for the production of wind power: overestimation and underestimation costs. The formulas for underestimating and overestimating costs can be stated as follows

$$E_{wnd,Z,T} = C_{wnd,z}(wnd_{R,Z} - wnd_{z,T})\left\{\exp\left(-\left(\frac{vl_{in,Z}}{S_{f,Z}}\right)^{S_{h,z}}\right) - \exp\left(-\left(\frac{vl_{out,Z}}{S_{f,Z}}\right)^{S_{h,z}}\right)\right\} + \left\{\exp\left(-\left(\frac{vl_{in,Z}}{S_{f,Z}}\right)^{S_{h,z}}\right) - \exp\left(-\left(\frac{vl_{out,Z}}{S_{f,Z}}\right)^{S_{h,z}}\right)\right\}\left\{wnd_{T,Z} + \frac{wnd_{R,Z}vl_{in,z}}{v_{in,Z} - v_{out,Z}}\right\} + \tau\left\{\left(\frac{1}{S_{h,Z}}\left(\frac{vl_{in}}{S_{f,Z}}\right)^{S_{h,Z}}\right) + 1\right\} + \tau\left\{\left(\frac{1}{S_{h,Z}}\left(\frac{vl_{R,Z}}{S_{f,Z}}\right)^{S_{h,Z}}\right) + 1\right\}\frac{wnd_{R,Z}vl_{in,z}}{v_{in,Z} - v_{out,Z}} \quad (8)$$

The "direct cost of wind power" or the money spent buying electricity from a wind farm operator in response to a specific demand, is expressed as follows

$$E_{dr.Z.T} = wnd_{Z.T} \times g_Z \quad (9)$$

Thus, the following are the wind power production estimates for each period, which considers the potential for under and overestimation, as well as the direct cost of wind generation

$$E_{wnd\_tot}=\sum_{z=1}^{N_{wnd}}\sum_{t=1}^{T_{hor}}\left(E_{dr.Z.t}+E_{UN.Z.t}+E_{OVR.Z.t}\right) \quad (10)$$

where N_{wnd} is the total number of wind generators.

2.2 Solar energy and its cost of production

In a solar power plant, the amount of energy produced is proportional to the amount of incoming solar radiation (SI_s) and the surrounding temperature (T_{amb}). Consequently, the solar energy output may be written as

$$SP_{solar}=SP_{solar}\times\frac{SI_s}{1\,000}\times\left\{\alpha_S\left(T_{ref}-T_{amb}\right)+1\right\} \quad (11)$$

The total solar share (S_{tot}) from the units that have been placed may be regulated by whether or not the solar panels are turned ON or OFF.

$$S_{tot}=\sum_{solar=1}^{ns}SP_{solar,t}\times U_{solar,t} \quad (12)$$

The solar share, denoted by S_{tot}, has a maximum limit that is capped at x_{solar}% of the total demand power at any sub-interval t within the total interval T, and the method for determining that limit can be expressed in mathematical terms as follows

$$S_{tot}\leqslant x_{solar}\times PD_t \quad (13)$$

To obtain the greatest advantage from the installed solar capacity, clients are assessed a penalty factor. Therefore, the cost of the difference between the installed power capacity and amount of solar power produced is as follows

$$F_{solar}=\sum_{t=1}^{T}\sum_{solar=1}^{ns}SP_{solar,t}\times PU_{cost_{solar}} \quad (14)$$

$$F_{solar}=\sum_{t=1}^{T}\sum_{solar=1}^{ns}\left(SP_{solar,t}-S_{solar,t}\right) \quad (15)$$

2.3 The economics of producing electricity from hydropower

Compared with other forms of power generation, the costs associated with operating a hydropower plant are minimal [26-27]. Combining a hydropower-producing unit with a thermal power plant is a viable option to reduce fuel and pollution costs [28]. Production of hydroelectric power, denoted by $PHY_{i,t}$, may be expressed in terms of water flow rate and reservoir capacity as follows

$$PHY_{i,t}=\mathrm{HO}_{6,i}+\mathrm{HO}_{5,i}\mathrm{disq}_{i,t}+\mathrm{HO}_{4,i}\mathrm{Vol}_{i,t}+\mathrm{HO}_{3,i}\mathrm{disq}_{i,t}\mathrm{Vol}_{i,t}+\mathrm{HO}_{2,i}\mathrm{Vol}^2_{i,t}+\mathrm{HO}_{1,i}\mathrm{disq}^2_{i,t} \quad (16)$$

where $\mathrm{HO}_{1,i}$, $\mathrm{HO}_{2,i}$, $\mathrm{HO}_{3,i}$, $\mathrm{HO}_{4,i}$, $\mathrm{HO}_{5,i}$ and $\mathrm{HO}_{6,i}$ are the coefficients for hydroelectric power generating units, and $\mathrm{Vol}_{i,t}$ and $\mathrm{disq}_{i,t}$ represent the water volume of the ith unit and discharge rate water of ith unit, respectively [29].

2.4 Generation of thermal electricity and its associated costs

The valve-point effect and quadratic function are often used to illustrate how a thermal power generator operates, as follows [30-31]

$$F_{Th\_tot}=\sum_{t=1}^{T}\sum_{i=1}^{N_{genTH}}\left(\alpha_i P_{th_i}^2+\beta_i P_{th_i}+\gamma_i+\left|e_{1i}\sin\left(e_{2i}(-P_{th\min_i}+P_{th_i})\right)\right|\right) \quad (17)$$

where the total number of thermal units is given by N_{genTH}; α_i , β_i , and γ_i are the fuel coefficients; e_{1i} and e_{2i} are the valve point loading effect constants; and $P_{th\min_i}$ is the lowest active power production of the ith thermal unit. Thus, the active power production cost for the thermal unit, along with the solar, wind, and hydro units, may be calculated as follows

$$F_{gen\_tot}=F_{solar}+E_{wnd\_tot}+F_{Th\_tot}+\gamma_w\sum_{t=1}^{H}\sum_{i=1}^{N_{genHY}}PHY_{i,t} \quad (18)$$

where the scalar constant γ_w maps water volume discharge to the price of generating an equal amount of electricity [32-34].

2.5 Formulation of the ATC and RES-thermal scheduling issue

In this study, the OPF concept is used to address the challenges faced by ATC. A target function or cost function is created to maximize electricity transmission from a source region of generating units to a sink region of loads through a network of transmission or tie lines without breaching the limits and restrictions imposed by the operation of the power grid. The thermal limit of a power line is the maximum power that can be transmitted across it. The purpose is to develop a mathematical formulation of the ATC cost function. Unlike most cases in which only the cost of producing power is considered, both the ATC and power generation cost (PGC) are considered here. This study focused on three major situations.

(1) Case A: Schedule RES with thermal units strategically to minimize the cost of active power

production [35-37].

(2) Case B: Maximize ATC without exceeding restraints imposed by the electrical system.

(3) Case C: Maximize ATC while minimizing the cost of producing electricity from RES (multi-objective).

Therefore, the cost function may be expressed as

$$F_{Tot} = \phi_{TL} F_{TL} + \phi_{TLA} F_{TLA} + \phi_V F_{Vmis} + \phi_{gen} F_{gen\_tot} \quad (19)$$

For the objective function, ϕ_{TL}, ϕ_V, ϕ_{TLA}, and ϕ_{gen} are positive scalar values. Using these scalar factors, a single or multi-objection cost function may be produced with appropriate weighting. Power flow through certain lines can be increased to improve ATC, as indicated below

$$F_{TLA} = \left| \frac{1}{S_{TLi} - S_{TLB_i}} \right| \quad (20)$$

where S_{TLi} is the power flowing down the ith line and S_{TLB_i} is the base power flowing along the line. A mathematical safeguard against transmission line overload has been included into the cost function in the form of the following if statement $S_{TL\max i} < S_{TLi}$ true

$$F_{TL} = \sum_{i=1}^{N_{TL}} \left(S_{TL\max i} - S_{TLi} \right)^2 \quad (21)$$

The following is the equality requirement placed on load flow

$$Q_{G_i} - Q_{D_i} - \sum_{j=1}^{N_{BUS}} V_i Y_{ij} V_j \sin(\theta_{ij} + \delta_j - \delta_i) = 0 \quad (22)$$

The following are the limits placed on the production of voltage, active power, and reactive power

$$V_i^{\min} \leqslant V_i \leqslant V_i^{\max} \quad i = 1, \cdots, N_{BUS} \quad (23)$$

$$P_{Gi}^{\min} \leqslant P_{Gi} \leqslant P_{Gi}^{\max} \quad i = 1, \cdots, N_{GEN} \quad (24)$$

$$Q_{Gi}^{\min} \leqslant Q_{Gi} \leqslant Q_{Gi}^{\max} \quad i = 1, \cdots, N_{GEN} \quad (25)$$

where N_{BUS} and N_{GEN} are the total bus and generator bus counts, respectively. $V_i^{\max}$, $P_{Gi}^{\max}$, and $Q_{Gi}^{\max}$ are the maximum and lowest voltages and active and reactive power production limitations, respectively, in the IEEE test system. The test system's tap setting transformer and shunt reactor compensations are as follows

$$T_i^{\min} \leqslant T_i \leqslant T_i^{\max} \quad i = 1, \cdots, N_T \quad (26)$$

$$Q_{SHi}^{\min} \leqslant Q_{SHi} \leqslant Q_{SHi}^{\max} \quad i = 1, \cdots, N_{SH} \quad (27)$$

where N_{SH} and N_T are the total number of shunt reactors and tap-transformers, respectively. Their minimum and maximum values are denoted by the superscripts min and max, respectively. The values of the scalar constants used in Eq. (19) are provided in Tab. 1, in which the scalar factor varies depending on the specifics of the case.

Tab. 1 System parameters

Case	ϕ_{TL}	ϕ_V	ϕ_{TLA}	ϕ_{gen}
Case A	1 000	1 000	0	1
Case B	20	20	10	0
Case C	20	20	10	0.001

3 Implementing the proposed algorithms

This section discusses several metaheuristic algorithms developed to address these issues, such as the proposed CSHO.

3.1 Incorporating the BBO algorithm

Biogeography studies the emergence of novel species, movement of populations from one ecosystem to another, and extinction of populations elsewhere. In BBO, a habitat is conceptualized as an island (region) separated from other islands by physical distance. To qualify as an ideal residential location, a habitat must have a high habitat suitability index (HSI). Suitability index variables (SIVs) are used to describe the factors that make space habitable [38]. The SIV index is assumed to be the habitat's independent variable, and thus the HSI is dependent on it. The basic BBO method for solving optimization problems comprises two steps migration and mutation [39].

3.1.1 Phase of migration

During the migration phase of BBO, characteristics migrate to other islands and emigration from the population occurs, resulting in creation of the next set of solutions. Rates of emigration and immigration from and to the *k*th island may be modelled as shown in Eqs. (28) and (29)

$$\lambda_k = I_{\max} \left(1 - \frac{S_k}{S_{\max}} \right) \quad (28)$$

$$\mu_k = \frac{E_m S_k}{S_{\max}} \quad (29)$$

where λ_k and μ_k are the immigration and emigration rates for the kth individual, respectively; $E_{\max}$, $I_{\max}$, and $S_{\max}$, represent for the kth individual's species count and the maximum number of species that may exist, respectively.

3.1.2 Phase of mutations

The BBO mutation process is meant to increase the population density to sustainably feed on excellent solutions. At this stage, the mutation rate determines the random change in the habitat SIV index [40]

$$mu_k = mu_{\max}\left(\frac{1-P_k}{P_{\max}}\right) \tag{30}$$

Each of these potential habitats, or candidate solutions, is denoted by m SIVs (a vector), with each SIV consisting of the value of the associated control parameter and P_k as shown in Eq. (31)

$$P_k=\begin{cases}\mu_{(k+1)}\cdot P_{(k+1)}-(\lambda_k+\mu_k)\cdot P_k & S=0\\ \mu_{(k+1)}\cdot P_{(k+1)}-(\lambda_k+\mu_k)\cdot P_k+\lambda_{(k-1)}\cdot P_{(k-1)} & 1\leqslant S\leqslant S_{\max}-1\\ P_{(k-1)}\cdot\lambda_{(k-1)}-(\lambda_k+\mu_k)\cdot P_k & S=S_{\max}\end{cases} \tag{31}$$

3.2 Incorporating the GWO algorithm

In 2014, Mirjalili et al. [41-45] pioneered the implementation of the GWO. The algorithm addresses the mechanics of hunting and the democratic behavior of grey wolves living together in a pack in the wild. Grey wolves adhere to a very hierarchical and domineering social structure when they are in a pack. The order of the social dominance hierarchy is as follows.

(1) Alpha wolves (α) (a female and a male): the pack's highest-ranking leaders who make the decisions.

(2) Beta wolves (β): subordinate wolves who assist the alpha.

(3) Delta wolves (δ): responsible for relaying information to the higher two tiers.

(4) Omega wolves: the lowest level in the wolf hierarchy that comprises infant and weak wolves who relay information to all other ranks.

This social order, which comprises tracking, surrounding, and attacking prey, can be mathematically modelled as discussed in the following section.

3.2.1 Rank in society

The optimal solution is designated as an alpha wolf (alpha), the second-best as a beta wolf (beta), and the third-best as a delta wolf (delta). The remaining candidate solution sets are assumed to be omega (omega). Although this described method, which is similar to a hunting mechanism, is mostly controlled by alpha, beta and delta also have an effect.

3.2.2 Phase of encircling prey

The surroundings of the prey that successfully use the hunting mechanism may be mathematically defined as follows

$$\boldsymbol{D}=\left|\boldsymbol{C}\cdot\boldsymbol{X}_p(t_0)-\boldsymbol{X}_w(t_0)\right| \tag{32}$$

$$\boldsymbol{X}_w(t_0+1)=\boldsymbol{X}_p(t_0)-\boldsymbol{A}\cdot\boldsymbol{D} \tag{33}$$

$$\boldsymbol{A}=2a\cdot\boldsymbol{rand}_1-a \tag{34}$$

$$\boldsymbol{C}=2\cdot\boldsymbol{rand}_2 \tag{35}$$

$$\boldsymbol{D}_i=\left|\boldsymbol{C}_i\cdot\boldsymbol{X}_i-\boldsymbol{X}_w\right| \tag{36}$$

where t_0 is the current iteration; $\boldsymbol{X}_p$ and $\boldsymbol{X}_w$ are the position vectors for a prey and a grey wolf, respectively; $\boldsymbol{C}$ and $\boldsymbol{A}$ are coefficient vectors; $\boldsymbol{rand}_1$ and $\boldsymbol{rand}_2$ are two different random vectors in between [0, 1]; and a is linearly reduced from 2 to 0 over the progress of said iterations. The three best solutions ($\boldsymbol{X}_{p\alpha}$, $\boldsymbol{X}_{p\beta}$, and $\boldsymbol{X}_{p\delta}$) are saved including the latest positions of the omegas according to the current best position. The final position, $\boldsymbol{X}_w(t_0+2)$ is defined by the positions of alpha, beta, and delta in the search space.

$$\boldsymbol{X}_1=\boldsymbol{X}_i-\boldsymbol{A}_1\left(\boldsymbol{D}_i\right) \tag{37}$$

$$\boldsymbol{X}_w(t_0+1)=\frac{1}{3}\left(\boldsymbol{X}_1+\boldsymbol{X}_2+\boldsymbol{X}_3\right) \tag{38}$$

where i is α. Similarly $\boldsymbol{X}_2$ and $\boldsymbol{X}_3$ can be evaluated by replacing i as β and δ, respectively.

During the course of the simulation, the alpha, beta, and delta wolves each make an educated guess on the location of the prey. If $\boldsymbol{A}>1$, then the candidate solutions have moved away from the prey, and if $\boldsymbol{A}<1$, then the candidate solutions have moved closer to the prey.

3.3 Incorporating the SHO algorithm

The SHO method is concerned with how a prey animal (within a herd) might improve its chances of surviving a predator assault; however, it does not consider how

this would affect the chances of surviving prey animals [46].

3.3.1 Phase of initializing the population

The first phase of the SHO algorithm involves random construction of predators and prey. During initialization, the total size of the A of N population is set to $A=a_1, a_2, \cdots, a_i, \cdots, a_N$, where a_i is the position of an individual. Each n-dimensional search space solution is $a_{i,j}=[a_{i,1}, a_{i,2}, \cdots, a_{i,n}]$. The initial population is produced randomly as follows

$$a_{i,j}^0=rand(0,1)\cdot\left(x_j^{UP}-x_j^{LW}\right) \tag{39}$$

where x_j^{UP} and x_j^{LW} denote the upper and lower limit of the jth dimension, respectively, and $rand(0, 1)$ is a random value between 1 and 0. The SHO method considers two distinct groups of search agents: the predatory pack ($P=\{p_1, p_2,\cdots, p_{NP}\}$), and the more peaceful herd ($H=\{h_1, h_2,\cdots, h_{NH}\}$). It has been noted that, in the wild, 90% to 70% of a population may be classified as a herd. As a result, we may write NH and NP as

$$NP=-NH+N \tag{40}$$

$$NH=floor(rand(0.7,0.9)\times N) \tag{41}$$

3.3.2 Survival value assignment stage

Notably, when predators and prey interact, each member of a pack or herd has a unique survival profile, and thus, a unique likelihood of surviving an attack or killing a target animal. The mathematical representation of this survival value SV_{a_i} for each individual animal in n-dimensional search space is as follows

$$SV_{a_i}=\frac{-f_{best}+f(a_i)}{f_{best}-f_{worst}} \tag{42}$$

where f_{best} and f_{worst} are the best and worst fitness values recorded thus far depending on the pace of convergence.

3.3.3 A selfish herd's structure

There are a few distinct positions within a herd's hierarchy. During aggregation, the herd leader controls the direction of the prey. Many members of a herd decide where to go based on their shared knowledge of how to stay alive and the proximity of other members of the herd. Those who abandon the herd choose their own path independent of the rest of the quarry.

3.3.4 Operators of herd movements

The SHO method is regulated by two distinct evolutionary theories. One set of leaders in the herd functions as the operator of the herd's movement, whereas another set of leaders in the herd acts as the operator of desertion and follows the movement. All animals in a selfish herd learn crucial details about one another during these operational movements, such as how far away they are from other members of the aggregation and the value of their own survival.

3.3.5 Operators of predator movement

The danger of predation for solitary individuals is greater than that for herd members. Mass motion causes a predator to become disoriented and misjudge where to launch an assault. An SHO model predicts how a predator's pack will travel in relation to a herd based on how well its members will be able to avoid being killed by the herd and how far away from it they are when the attack begins.

3.3.6 Probabilities of pursuing

In SHO, the equation for the pursuit probability is

$$\rho_{p_i,h_j}=\frac{\gamma_{p_i,h_j}}{\sum_{m=1}^{NH}\gamma_{p_i,h_m}} \tag{43}$$

where γ_{p_i,h_j} are the degrees to which h_j and p_i are interested in the prey. At the kth iteration, the following equation is used to change the position of the predator

$$p_i^{1+k}=2\cdot rand(0,1)\left(h_r^k-p_i^k\right)+p_i^k \tag{44}$$

where h_r^k is a member of the herd that was picked at random during the kth iteration of the process.

3.3.7 Period of predation

In the SHO technique, the predation phase determines how the prey and predator interact. It is thought that after both the pack of predators and the selfish herd (prey) move, the exclusion of a solution from the current set of solutions and the dangerous area can be shown as follows for n-dimensional space

$$R=\frac{\sum_{j=1}^{n}x_j^{UP}-x_j^{LW}}{2\times n} \tag{45}$$

3.3.8 Period of restoration

Predation causes the size of prey populations to change dynamically throughout the year. This effect is reflected in the manner in which the SHO algorithm returns the number of prey items. By replacing the members of the herd who were kicked out and letting

them mate, the original balance of the herd's population is restored.

3.4 An introduction of chaotic maps

In this section, the authors describe their devised hybrid SHO algorithm, which uses the idea of a chaotic scale factor. In a chaotic system, the most important concerns are the preliminary factors and sensitivity of the conditions. The process of initializing the SHO algorithm has been significantly aided by the chaos concept. Therefore, to achieve better convergence, a hybridization of chaos and SHO is proposed in this study. According to previous papers [47-48], chaotic combinations are often nonlinear stimulation systems. Therefore, the response of chaotic combinations depends on both the changes in the system parameters and the starting expressions. Numerous chaotic map iterations have been proposed. In this article, ten distinct chaotic maps were considered. These maps are as follows: circle, cubic, logistic, Gaussian/mouse, iterative, sinusoidal, sine, singer, tent, and piece-wise [49]. A quick tabulation of these maps is presented in Tab. 2. After combining the above ten chaotic maps with the SHO algorithms to create an initial SHO population for resetting the simulation, the optimal chaotic map was chosen for use in the IEEE 9-bus, IEEE 39-bus, and Northern Regional Power Grid (NRPG) 246-bus systems.

Tab. 2 Names of the different chaotic maps and their mathematical expressions

Sl No.	Name of map	Chaotic map equation
COM1	Circle map	$x_{n+1}=\mathrm{mod}\left(x_n+B\left(\frac{A}{2\pi}\right)\sin\left(2\pi x_n\right),1\right)$
COM2	Cubic map	$x_{n+1}=Ax_n\left(1-x_n^2\right)$
COM3	Logistic map	$x_{n+1}=Ax_n\left(1-x_n\right)$
COM4	Mouse/Gussian map	$x_{n+1}=\begin{cases}1 & x_n=0\\ \dfrac{1}{\mathrm{mod}\left(x_n,1\right)} & \text{Otherwise}\end{cases}$
COM5	Iterative map	$x_{n+1}=\sin\left(\frac{A\pi}{x_n}\right)$
COM6	Sine map	$x_{n+1}=\frac{A}{4}\sin(\pi x_n)$
COM7	Sinusoidal map	$x_{n+1}=Ax_n^2\sin\left(\pi x_n\right)$
COM8	Singer map	$x_{n+1}=1.07\left(7.86x_n-23.31x_n^2+28.75x_n^3-13.302\,87x_n^4\right)$
COM9	Piece-wise map	$x_{n+1}=\begin{cases}\dfrac{x_n}{P} & 0\leqslant x_n\leqslant P\\ \dfrac{x_n-P}{0.5-P} & P\leqslant x_n<0.5\\ \dfrac{1-x_n-P}{0.5-P} & 0.5\leqslant x_n<1-P\\ \dfrac{1-x_n}{P} & 1-P\leqslant x_n<1\end{cases}$
COM10	Tent map	$x_{n+1}=\begin{cases}\dfrac{x_n}{0.7} & x_n<0.7\\ \dfrac{10}{3}\left(1-x_n\right) & x_n\geqslant 0.7\end{cases}$

3.5 Issues with CSHO implementation

In this section, the implementation of the proposed hybrid chaotic SHO is explored using the flowchart shown in Fig. 1. In a previously described technique, the SHO-COM5 A chaotic map is interchangeable with several other possibilities. As presented in Tab. 3, SHO-COM5 was used in this study.

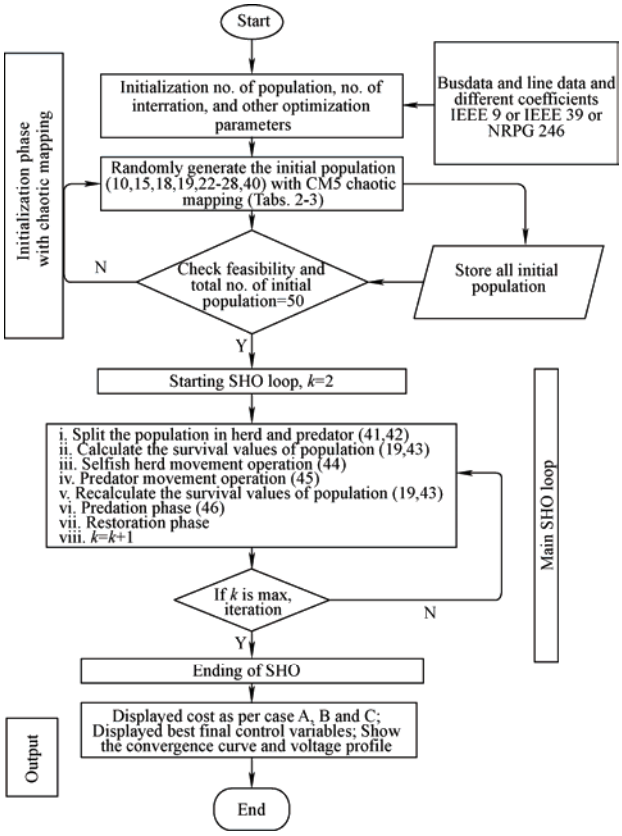

Fig. 1 Flow chart of CSHO

Tab. 3 The chaotic map results for Case A using the 9-bus system

Chaos	Min	Average	Max
SHO-COM1	16 121.505 1	16 121.501 4	16 136.469 7
SHO-COM2	16 132.793 6	16 122.718 5	16 134.849
SHO-COM3	16 114.133 6	16 127.206 8	16 128.826 8
SHO-COM4	16 116.570 7	16 121.659 1	16 124.529 6
SHO-COM5*	16 113.773 5	16 121.258 4	16 124.518 3
SHO-COM6	16 121.192 2	16 142.275 7	16 141.282 6
SHO-COM7	16 123.212 2	16 128.698 3	16 124.593 6
SHO-COM8	16 133.969 7	16 124.977 7	16 125.522 2
SHO-COM9	16 124.927 3	16 121.346 1	16 135.127 9
SHO-COM10	16 129.204 3	16 122.621 2	16 130.066 3

4 Case studies and observations

In this study, three different test systems were used to assess the efficacy of the recommended algorithms: IEEE 9-bus, IEEE 39-bus [50-51], and NRPG 246-bus [52] systems. Each of these test systems had a different number of buses. Thirty trial runs were performed for each test case and each optimization, utilizing data from the MATPOWER toolkit and other sources [50-55]. Fifty individuals were chosen randomly from the entire population to represent each incident. All test cases were implemented on a system made by ASUS with a Ryzen 5 processor running at a speed of 2 GHz, Windows 10 (Home, 64 bits), 12 GB of RAM (DDR3) memory, and Matlab 2020a. In this study, 30 random trial runs were performed on a 9-bus system to generate ten different chaotic map variants for Case A. A comparative analysis is shown in Tab. 3. Compared with other chaotic maps of hybridization, the iterative chaotic map, also known as COM5, provides the most desirable results when used in conjunction with SHO. Therefore, an iterative chaotic map hybridization with SHO was considered for all examples utilized in this study. A standard MVA of 100 was used for the calculations.

4.1 Research and findings of the 9-bus test system

In the 9-bus test system, there are nine buses and six generating units; two are hydro units, one is a wind unit, two are solar units (consisting of 13 panels each), and one is a thermal unit. The 9-bus test system was designed to simulate real-world conditions. The active and reactive loads are denoted as (PD1, PQ1), (PD2, PQ2), and (PD3, PQ3), respectively, and tabulated for a 24 h load, as shown in Tab. 4. There were three load buses: buses 5, 7, and 9. In this study, the ATC computation is performed using line number 2, which extends from bus 4 to bus 5. In the IEEE 9-bus test system, the control variables consisted of two discharges for two hydro units, active power generation from one thermal unit, active power generation from one wind unit, and active power generation from two solar generation units, six generating bus voltages, two taps that set the transformer tap positions, and two shunt compensation Vars. Consequently, the total number of control variables was 16. Subsequently, three instances were investigated in chronological order. The authors' primary goal in the first scenario, which they refer to as Case study A, was to reduce the cost of generation to the maximum possible extent. Tab. 4 shows the active and reactive power demands round the clock for 9 bus. As shown in Tab. 5, the reduction in total cost after 30 random trial runs using BBO was determined to be \$16 147.286 5/24 h, which is superior to that achieved using a sine cosine algorithm (SCA) in conjunction with economic load scheduling, \$18 268.570/24 h [50]. Moreover, GWO yields better results for the same \$16 142.562 3/24 h, whereas the proposed algorithm in conjunction with the COM5 method yields the best result of \$16 113.773 5/24 h. Tab. 6 shows the demand for 39 bus system. It is also noteworthy that in this case, the total thermal cost is reduced to \$11 851.649 3/24 h, and the control parameters for these test studies, including water discharge, wind and thermal generation, six generating bus voltages, two tap-setting transformers, and two shunt capacitors injected with Var and two solar units (panel-wise states), for 24 h are provided in Tab. 7.

Tab. 4 Demand in the PU of a 9-bus system that is active and reactive round the clock

Hour	PD1	PD2	PD3	PQ1	PQ2	PQ3
1	0.900	1.000	1.250	0.300	0.350	0.500
2	0.936	1.040	1.300	0.312	0.364	0.520
3	0.840	0.933	1.160	0.280	0.327	0.467
4	0.780	0.867	1.080	0.260	0.303	0.433
5	0.804	0.893	1.117	0.268	0.313	0.447
6	0.960	1.067	1.333	0.320	0.373	0.533
7	1.140	1.267	1.583	0.380	0.443	0.633
8	1.212	1.347	1.683	0.404	0.471	0.673
9	1.308	1.453	1.817	0.436	0.589	0.727
10	1.296	1.440	1.800	0.432	0.504	0.720
11	1.320	1.467	1.833	0.440	0.513	0.733
12	1.380	1.533	1.917	0.460	0.537	0.767
13	1.332	1.480	1.850	0.444	0.518	0.740
14	1.236	1.373	1.717	0.412	0.481	0.687
15	1.212	1.347	1.683	0.404	0.471	0.673
16	1.272	1.413	1.767	0.424	0.495	0.707
17	1.260	1.400	1.750	0.420	0.490	0.700
18	1.344	1.493	1.867	0.448	0.523	0.747
19	1.284	1.427	1.783	0.428	0.499	0.713
20	1.260	1.400	1.750	0.420	0.490	0.700
21	1.092	1.213	1.517	0.364	0.425	0.607
22	1.032	1.147	1.433	0.344	0.401	0.573
23	1.020	1.130	1.417	0.340	0.397	0.567
24	0.960	1.067	1.333	0.320	0.373	0.533

Tab. 5 Maximization of savings by comparing costs over 24 h and 9-bus using various approaches

Cases	Methods	Mini. total fitness cost	Ave. total fitness cost	Worst total fitness cost	ATC (24 h)	Only generation cost/$	Thermal generation cost/$	Wind cost/$	Solar cost/$	Line flow violation	No. of trial	Simulation time/s
Case A: Only PGC optimization	SCA-ELS[50]	18 268.57	NA	NA	NA	18 268.57	NA	NA	NA	NA	NA	19
	BBO	16 147.29	16 154.75	16 160.65	0.018 4	16 147.29	12 433.41	3 067.984	645.891 5	0	30	28
	GWO	16 142.56	16 149.56	16 153.82	0.019 1	16 142.56	12 268.35	3 228.513	645.702 5	0	30	22
	SHO	16 135.86	16 142.65	16 146.51	0.019 8	16 135.86	12 101.89	3 752.329	281.635 2	0	30	15
	CSHO	16 113.77	16 121.26	16 124.52	0.019 3	16 113.77	11 851.65	3 593.671	668.453 6	0	30	17
Case B: Only ATC optimization	BBO	265.235 8	271.819 8	277.442 8	0.037 7	18 952.24	11 769.34	6 633.283	549.614 8	0	30	24
	GWO	263.254 7	268.669 7	272.924 5	0.038	18 951.59	12 697.56	5 685.476	568.547 6	0	30	18
	SHO	260.458 1	263.673 1	266.923 1	0.038 4	18 952.55	11 940.1	6 443.866	568.576 4	0	30	15
	CSHO	256.647 1	259.862 1	262.874 5	0.039	18 950.08	11 289.36	6 999.504	661.217 8	0	30	16
Case C: Multi-objective	BBO	272.106 5	277.455	286.330 4	0.039 9	21 354.24	13 666.71	7 046.898	640.627 1	0	30	33
	GWO	267.344 9	271.599 7	277.475 1	0.040 6	20 857.33	13 765.83	6 465.771	625.719 8	0	30	28
	SHO	254.543 5	258.092 2	261.967 6	0.042 6	19 636.25	12 959.93	6 087.239	589.087 6	0	30	25
	CSHO	240.243 2	242.597 8	245.166 5	0.045 2	19 234.25	12 359.31	6 291.21	583.731 3	0	30	23

Tab. 6 PU demand of a 39-bus system that is active and reactive round the clock

Hr.	H-factor	Hr.	H-factor	Bus	Base P_d	Base Q_d	Bus	Base P_d	Base Q_d	Bus	Base P_d	Base Q_d
1	0.438	14	0.518	1	0	0	14	0	0	27	2.81	0.755
2	0.422	15	0.542	2	0	0	15	3.2	1.53	28	2.06	0.276
3	0.394	16	0.479	3	3.22	0.024	16	3.29	0.323	29	2.835	0.269
4	0.315	17	0.505	4	5	1.84	17	0	0	30	0	0
5	0.434	18	0.622	5	0	0	18	1.58	0.3	31	0.092	0.046
6	0.413	19	0.688	6	0	0	19	0	0	32	0	0
7	0.457	20	0.635	7	2.338	0.84	20	6.8	1.03	33	0	0
8	0.51	21	0.599	8	5.22	1.766	21	2.74	1.15	34	0	0
9	0.5	22	0.489	9	0.065	–0.666	22	0	0	35	0	0
10	0.494	23	0.433	10	0	0	23	2.475	0.846	36	0	0
11	0.484	24	0.444	11	0	0	24	3.086	–0.922	37	0	0
12	0.524	—	—	12	0.085	0.88	25	2.24	0.472	38	0	0
13	0.564	—	—	13	0	0	26	1.39	0.17	39	11.04	2.5

Tab. 7 Parameters for maximizing CSHO's cost-effectiveness in a 9-bus system sole generator (PGC)

Hr.	Discharge 1	Discharge 2	Thermal 1/p.u.	Wind 1/p.u.	V_{g1}/ p.u.	V_{g2}/ p.u.	V_{g3}/ p.u.	V_{g4}/ p.u.	V_{g5}/ p.u.	V_{g6}/ p.u.	TR_1	TR_2	QC_1/ p.u.	QC_2/ p.u.	P_{total1}	P_{total2}	Solar unit$_s$	Solar unit$_2$
1	0.57	1.47	1.52	0.25	0.97	1.09	0.91	1.02	0.97	0.91	1.06	0.99	0.04	0.03	0.00	0.00	0000000000000	0000000000000
2	1.24	1.50	1.61	0.00	0.97	1.03	1.01	1.03	0.91	0.97	1.05	0.95	0.01	0.00	0.00	0.00	0000000000000	0000000000000
3	0.60	0.60	1.86	0.03	0.94	1.04	0.99	1.04	1.03	0.97	1.04	0.97	0.04	0.00	0.00	0.00	0000000000000	0000000000000
4	0.82	1.25	1.09	0.06	1.01	0.98	1.04	1.01	0.95	1.04	0.99	0.94	0.03	0.01	0.00	0.00	0000000000000	0000000000000
5	0.80	1.36	0.88	0.35	0.98	0.91	1.03	1.04	0.93	1.00	0.97	0.91	0.00	0.04	0.01	0.01	0000000111011	1000000000101
6	0.80	1.22	0.86	0.45	0.92	1.01	0.91	0.98	0.99	1.00	0.92	0.96	0.04	0.02	0.21	0.27	0100100001011	1010110011011
7	0.70	1.43	1.32	0.09	1.08	1.08	0.92	0.96	1.09	1.09	0.92	1.04	0.00	0.01	0.45	0.61	0111010000110	0100111000111
8	0.66	0.60	0.76	0.15	0.92	0.94	1.02	1.04	0.97	0.99	0.97	0.94	0.01	0.04	1.10	1.13	0010101000111	0001101101100
9	0.50	1.30	0.73	0.52	1.02	0.92	0.92	1.04	0.91	1.03	1.02	1.01	0.01	0.04	0.43	1.53	0110000000010	1101110110101
10	0.50	1.27	0.59	0.26	0.94	0.98	0.95	1.08	1.06	1.03	0.91	1.05	0.02	0.03	1.38	0.92	0101001101010	1001000001100
11	0.70	1.31	0.13	0.21	0.94	0.98	0.95	1.07	1.07	1.01	0.96	0.93	0.03	0.03	0.46	2.30	0101000000000	0001001011011
12	0.58	1.34	0.16	0.17	0.92	0.99	1.04	0.96	0.98	0.91	1.07	1.02	0.04	0.01	1.54	1.60	0110110000010	0000100011010
13	0.76	1.34	0.11	0.02	1.00	1.10	1.03	0.94	1.08	0.96	0.93	1.01	0.01	0.04	1.67	1.33	0010001100110	0010010010010
14	0.98	1.25	0.19	0.16	1.01	1.05	1.00	0.95	0.91	1.03	0.94	0.95	0.02	0.01	0.84	1.44	0001000001010	1000000011011
15	0.56	1.49	0.66	0.05	1.06	0.93	0.99	0.94	1.10	0.91	1.04	0.97	0.04	0.03	1.26	0.75	0111000100001	0001000100010
16	0.50	1.48	0.34	0.31	1.06	1.01	0.93	0.94	1.05	1.00	0.92	1.08	0.02	0.01	1.28	1.07	0111110001010	0100100011001
17	0.57	1.40	1.50	0.30	0.99	0.99	0.93	0.91	1.01	0.96	1.02	0.90	0.00	0.01	0.64	0.40	0100001011100	0001000011000
18	0.50	1.22	2.09	0.33	1.01	1.06	0.96	1.02	1.04	0.92	1.04	1.09	0.04	0.02	0.49	0.38	0110000101101	0000100011101
19	0.60	1.41	2.56	0.18	1.02	1.01	1.00	0.93	1.06	1.01	0.99	0.91	0.01	0.04	0.09	0.09	0111110001110	0101101011010
20	1.31	1.34	2.28	0.12	0.96	1.01	0.98	0.97	0.99	1.04	0.93	0.90	0.05	0.03	0.00	0.00	0000000000000	0000000000000
21	0.50	1.49	2.07	0.26	0.98	1.00	1.07	1.09	0.94	0.99	1.09	0.91	0.04	0.01	0.00	0.00	0000000000000	0000000000000
22	0.76	1.33	1.69	0.16	1.10	1.09	1.05	1.09	0.99	0.94	1.07	1.04	0.01	0.05	0.00	0.00	0000000000000	0000000000000
23	1.50	1.38	1.29	0.17	0.93	1.09	1.05	0.92	1.02	0.94	0.90	1.05	0.00	0.02	0.00	0.00	0000000000000	0000000000000
24	1.50	1.42	1.23	0.02	1.04	0.95	0.93	1.06	0.94	1.06	1.09	1.00	0.05	0.01	0.00	0.00	0000000000000	0000000000000

Observations indicate that thirteen solar panels in each solar unit have two states, ON and OFF, represented by "1" and "0", respectively. Fig. 2 depicts the costs ($/24 h) of the various described algorithms for all instances and Fig. 3 shows a 3D picture of how the voltages of all nine buses changed over the course of 24 h. In scenario B (maximum ATC) for the suggested CSHO, the maximum values are 0.039 p.u. for 24 h, which is the best of the optimization strategies presented. Case study C concludes the discussion of multi-objective optimization by minimizing the total cost and maximizing the ATC. All controlled parameters are shown in Tab. 8. Again, the CSHO approach delivered the best results of $240 243.2/24 h compared to other suggested algorithms based on 30 separate trial runs, with all control parameters shown in Tab. 9. In Fig. 3, the voltage profiles of all nine buses are shown in 3D for all times in a 24-h period. In addition, Tab. 10 summarizes the lowest (best), average, and maximum (worst) production costs of other approaches for each case's 30 unique trial runs. The simulation results demonstrated the computational efficacy of the proposed CSHO method.

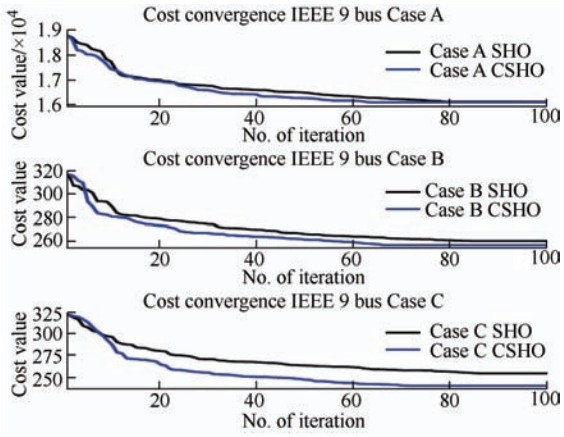

Fig. 2 The cost-effectiveness of the 9-bus system in a range of simulations

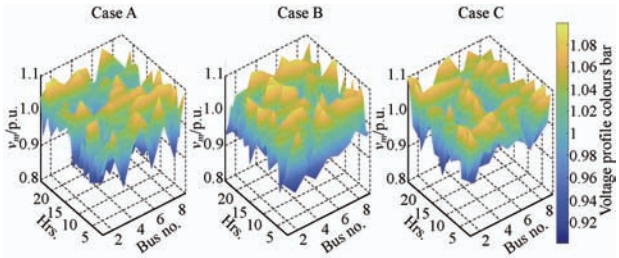

Fig. 3 Voltage across a 9-bus system subjected to a variety of stress conditions (Bus voltage of IEEE 9 bus: 24 h)

Tab. 8 All parameters for ATC optimization by CSHO for 9-bus system

Hr.	Discharge 1	Discharge 2	Thermal 1/p.u.	Wind 1 /p.u.	V_{g1}/ p.u.	V_{g2}/ p.u.	V_{g3}/ p.u.	V_{g4}/ p.u.	V_{g5}/ p.u.	V_{g6}/ p.u.	TR_1	TR_2	QC_1/ p.u.	QC_2/ p.u.	P_{total1}	P_{total2}	Solar unit$_s$	Solar unit$_2$
1	0.63	1.47	1.55	0.18	1.03	1.09	0.98	1.06	0.96	1.02	0.95	0.94	0.04	0.04	0.00	0.00	0000000000000	0000000000000
2	0.71	1.31	1.47	0.39	0.96	0.90	0.94	0.91	1.04	0.99	0.97	0.91	0.04	0.04	0.00	0.00	0000000000000	0000000000000
3	0.50	1.47	0.98	0.65	0.94	1.03	1.05	0.97	1.02	1.08	1.09	0.95	0.01	0.03	0.00	0.00	0000000000000	0000000000000
4	0.88	1.48	1.00	0.13	0.90	1.00	0.96	1.03	1.04	1.01	1.06	0.91	0.05	0.02	0.00	0.00	0000000000000	0000000000000
5	0.76	0.60	1.13	0.48	1.06	1.05	1.06	0.99	1.01	1.02	0.98	0.92	0.04	0.03	0.01	0.01	1111010100100	0000001000111
6	0.50	1.40	1.26	0.35	1.05	0.90	1.05	0.93	1.05	1.09	1.05	1.02	0.00	0.03	0.23	0.19	1001111101000	1101000010110
7	0.71	1.44	1.06	0.22	1.02	1.07	1.09	1.09	1.09	0.96	0.95	1.08	0.04	0.05	0.83	0.39	1111001111101	0111010001000
8	0.58	1.13	1.00	0.12	0.94	0.96	0.91	0.99	0.97	0.93	0.90	0.90	0.05	0.04	0.68	1.15	0100101000010	0100001010111
9	0.50	1.35	0.30	0.11	1.01	1.05	0.97	0.98	1.00	0.91	1.03	1.09	0.03	0.03	1.50	1.48	1101111010101	1110111010110
10	0.56	1.38	0.85	0.18	0.99	1.09	0.90	0.93	1.03	0.99	0.97	0.91	0.01	0.04	1.31	0.85	1101100000101	0000000011001
11	0.52	1.42	0.22	0.36	0.99	0.98	0.92	1.06	0.97	0.95	1.07	1.03	0.02	0.02	1.33	1.43	0110000000011	1000000000111
12	0.53	0.60	0.41	0.08	1.10	1.07	1.05	1.04	0.92	1.00	1.07	1.08	0.03	0.01	2.39	1.06	1010111001100	0100010010000
13	0.52	1.27	0.32	0.13	1.02	0.93	0.93	1.04	0.98	0.98	0.97	1.08	0.04	0.02	1.95	1.00	0110001010011	0100000000110
14	1.17	1.29	0.18	0.00	0.99	1.01	0.96	1.10	1.03	0.99	0.95	1.09	0.02	0.04	1.55	0.84	0110110110000	0010000001100
15	0.76	1.34	0.75	0.48	0.91	1.06	0.91	0.99	0.93	1.05	1.01	1.10	0.01	0.03	0.68	0.72	1000000100100	0001010100000
16	1.00	1.39	0.73	0.05	1.10	0.95	1.10	1.09	0.96	1.01	1.07	1.05	0.04	0.00	0.83	1.07	0100100011000	0010100100110
17	1.09	1.33	0.71	0.79	0.95	0.97	0.92	1.09	0.94	1.06	1.01	1.06	0.02	0.02	0.51	0.53	1000000110100	0010000011100
18	0.93	1.40	1.82	0.35	0.98	1.01	0.96	1.10	0.95	0.99	1.06	1.09	0.04	0.05	0.45	0.27	1010111100100	0100100010001
19	0.81	1.31	1.92	0.69	0.95	0.95	0.98	1.08	0.96	1.07	1.00	1.03	0.04	0.03	0.10	0.05	1010010101111	0110000100010
20	0.54	1.48	2.72	0.15	0.98	1.07	1.01	1.00	1.07	1.06	1.01	1.03	0.00	0.01	0.00	0.00	0000000000000	0000000000000
21	0.52	1.09	2.00	0.41	0.96	0.97	1.00	0.96	1.08	1.07	1.08	1.04	0.02	0.00	0.00	0.00	0000000000000	0000000000000
22	0.80	1.50	1.65	0.11	1.03	0.92	1.10	1.09	1.10	1.04	0.95	1.06	0.03	0.04	0.00	0.00	0000000000000	0000000000000
23	1.50	1.32	0.66	0.82	0.96	0.94	1.04	1.08	0.98	0.94	1.05	1.09	0.01	0.00	0.00	0.00	0000000000000	0000000000000
24	1.49	1.45	1.06	0.17	0.93	1.03	0.99	0.96	1.04	0.99	0.97	1.02	0.01	0.02	0.00	0.00	0000000000000	0000000000000

Tab. 9 For a 9-bus system, CSHO's full set of multi-objective optimization parameters

Hr.	Discharge 1	Discharge 2	Thermal 1 /p.u.	Wind 1 /p.u.	V_{g1}/ p.u.	V_{g2}/ p.u.	V_{g3}/ p.u.	V_{g4}/ p.u.	V_{g5}/ p.u.	V_{g6}/ p.u.	TR_1	TR_2	QC_1/ p.u.	QC_2/ p.u.	P_{total1}	P_{total2}	Solar unit$_1$	Solar unit$_2$
1	0.90	1.40	1.27	0.28	1.10	1.04	1.00	1.08	1.01	1.02	0.98	1.06	0.01	0.01	0.00	0.00	0000000000000	0000000000000
2	0.83	1.39	1.68	0.08	0.95	1.03	1.04	1.05	1.05	1.07	0.99	1.06	0.05	0.00	0.00	0.00	0000000000000	0000000000000
3	0.50	1.36	1.57	0.06	1.08	0.92	1.08	1.01	0.98	0.95	0.92	1.10	0.05	0.02	0.00	0.00	0000000000000	0000000000000
4	0.50	1.48	1.15	0.21	0.94	1.07	1.07	1.09	1.08	1.08	0.93	1.07	0.03	0.03	0.00	0.00	0000000000000	0000000000000
5	0.50	0.96	0.91	0.68	1.09	1.00	1.07	0.93	1.02	0.92	1.07	0.94	0.01	0.03	0.01	0.01	1001001101010	0100010101000
6	0.65	1.38	0.68	0.81	1.04	0.94	0.93	1.07	0.94	1.04	1.03	1.08	0.03	0.03	0.19	0.21	0110110000110	1000010110101
7	0.79	1.48	0.68	0.76	0.99	1.03	0.96	0.93	1.07	0.92	1.07	0.91	0.05	0.02	0.42	0.61	0100110100001	1000110100111
8	0.50	1.49	2.46	0.00	0.96	0.95	0.99	1.06	0.98	1.07	0.95	1.09	0.03	0.03	0.21	0.26	0000000001000	0110000000000
9	1.12	1.47	0.12	0.81	0.99	1.05	1.03	1.07	0.92	0.95	1.05	1.03	0.02	0.02	0.92	1.12	1110011000010	0111111000010
10	0.76	1.23	1.18	0.49	1.05	1.01	0.91	1.09	0.98	0.98	0.99	1.04	0.05	0.02	0.46	0.95	0100000100000	1000001100001
11	0.59	1.48	0.38	0.19	0.90	1.03	0.93	1.03	0.94	1.06	1.01	1.02	0.02	0.03	1.33	1.38	1001000110000	0010100010100
12	0.78	0.60	1.00	0.20	0.93	1.09	0.98	1.05	0.94	1.05	0.95	1.02	0.03	0.04	1.17	1.28	0001000000011	0000000110100
13	0.50	1.46	0.20	0.07	0.97	0.91	0.95	1.09	0.95	0.97	1.09	1.05	0.04	0.04	1.81	1.33	1100110110000	0010001011000
14	0.91	1.45	0.28	0.00	0.94	1.03	0.96	0.97	0.96	0.96	0.95	1.10	0.02	0.04	1.08	1.32	0011000100100	1010000101010
15	1.18	1.49	0.44	0.07	0.98	1.06	0.97	1.08	0.93	0.99	1.06	1.09	0.03	0.03	1.06	0.85	1010011000001	1001001010000
16	0.53	1.05	0.38	0.11	1.06	0.91	0.99	1.02	0.99	0.92	1.10	1.09	0.02	0.00	1.68	1.04	1011000111011	0101001100100
17	0.50	0.60	1.91	0.26	1.03	1.03	0.91	1.03	0.99	1.08	0.99	1.07	0.02	0.04	0.66	0.48	0100001011001	1000100001010
18	0.75	1.50	1.96	0.47	0.97	1.01	0.93	0.94	0.95	0.92	1.08	0.96	0.02	0.03	0.27	0.26	0101000110000	0010110000010
19	0.96	1.22	2.51	0.01	0.92	1.09	1.09	1.08	0.97	1.05	0.92	1.05	0.04	0.01	0.10	0.08	1110100011101	1111110100000
20	0.50	1.49	2.74	0.15	1.07	1.04	0.96	1.05	1.03	1.07	0.93	1.01	0.03	0.01	0.00	0.00	0000000000000	0000000000000
21	0.50	1.22	2.33	0.03	1.10	1.05	0.99	0.92	0.97	0.99	1.02	1.07	0.00	0.01	0.00	0.00	0000000000000	0000000000000
22	0.76	1.36	1.76	0.09	0.97	0.90	0.99	0.93	0.92	1.01	1.06	1.05	0.01	0.01	0.00	0.00	0000000000000	0000000000000
23	1.49	1.49	1.05	0.38	1.06	0.91	0.92	1.02	1.04	1.05	0.97	1.05	0.01	0.00	0.00	0.00	0000000000000	0000000000000
24	1.50	1.17	1.05	0.28	1.10	1.08	0.99	1.07	0.97	0.95	1.05	1.09	0.04	0.03	0.00	0.00	0000000000000	0000000000000

Tab. 10 Maximization of savings by comparing prices over 24 h with 39-bus using various approaches

Cases	Methods	Min. total fitness cost	Ave. total fitness cost	Worst total fitness cost	ATC / 24 h	Only generation cost/$	Thermal generation cost/$	Wind cost/$	Solar cost/$	Line flow violation	No. of trial	Simulation time/s
Case A: Only PGC optimization	BBO	352 661	352 663.4	352 665.7	0.078 5	352 665.7	351 255.1	1 181.43	229.232 7	0	30	42
	GWO	352 658.6	352 664.3	352 668.5	0.079 1	352 668.5	348 708	1 183.055	2 777.413	0	30	35
	SHO	352 653.4	352 656.6	352 659	0.079 1	352 659	349 097.2	1 147.757	2 414.099	0	30	32
	CSHO	352 651	352 653.4	352 655.7	0.081 4	352 655.7	350 366.6	1 277.044	1 012.071	0	30	30
Case B: Only ATC optimization	BBO	82.363 8	84.729 2	87.094 6	0.080 6	371 992.5	369 785.6	960.958 3	1 245.896	0	30	43
	GWO	77.127 3	79.492 7	83.858 1	0.137 6	371 990.1	369 781.2	1 007.617	1 201.237	0	30	34
	SHO	73.761 9	76.127 3	78.492 7	0.138 8	371 977.7	369 775.7	1 214.801	987.254 8	0	30	32
	CSHO	71.396 5	73.761 9	77.121 9	0.140 1	371 975.4	369 773.3	1 275.277	926.778 7	0	30	31
Case C: Multi-objective	BBO	518.623 1	524.981 1	529.982 1	0.066 2	367 445.3	365 146.3	1 385.329	913.677 3	0	30	33
	GWO	450.005 7	457.241 5	463.599 5	0.121	367 325.1	365 133.9	1 283.111	908.023 3	0	30	28
	SHO	448.422 1	453.986 1	456.351 1	0.123 2	367 244.9	364 998.8	1 340.475	905.658 3	0	30	25
	CSHO	447.509 8	449.875 2	454.975 2	0.124 4	367 144.8	364 975.7	1 275.596	893.538 3	0	30	23

4.2 Research and findings of the 39-bus test system

The 39-bus test system has 14 generating units: four hydro units, two wind units, two solar units (each consisting of 13 panels), and six thermal units. There are 39 buses in the system. There are 25 load buses with a total active base load demand of 61.566 p.u., total reactive base load demand of 13.429 p.u., and load demand over a period of 24 h varied according to the H factor, as shown in Tab. 4. Subsequently, three instances were investigated in chronological order. In the first case, the authors were only concerned with minimizing the cost of generation; in the second case, they were concerned with maximizing the ATC; and in the third case, they were concerned with minimizing the cost while also maximizing the ATC (a multi-objective problem). These three cases were designated as A, B, and C, respectively. Within the context of this study, the ATC calculation considers Line No. 9, which extends from Bus 4 to Bus 14. In the first scenario, called "Case A" by the authors, they focused only on lowering the cost of making electricity. According to Tab 10, the minimal total cost that may be achieved with BBO after 30 random trial runs is $352 660.989 5/24 h. In comparison, SHO delivers $352 653.383 19/24 h, whereas the suggested CSHO with CM5 delivered $352 651.017 8/24 h. Fig. 4 shows the convergence curves, which indicate how much better the suggested CSHO is than what is already being used. All produced bus voltage magnitudes are displayed in Fig. 5. Tabs. 11-13 show the control parameters under different case studies and the ON/OFF statuses of the solar units are listed in Tab. 14. Tab. 11 shows the discharges, thermal generation, and wind generation for the CSHO over the course of 24 h. Considering the suggested CSHO, the maximization of ATC produces the highest value of 0.140 1 p.u. for 24 h, which is the best among all optimization strategies covered in this study. The control parameters for the CSHO are listed in Tabs. 12 and 13, respectively.

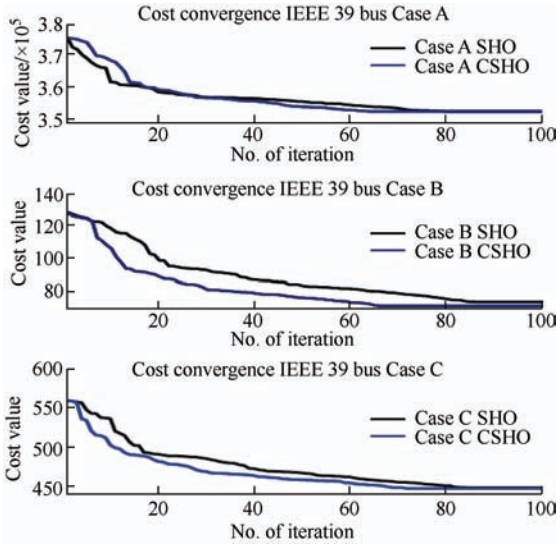

Fig. 4 Cost-effectiveness of a 39-bus system in a range of simulations

Tab. 11 Total cost minimization of discharge and active power production for CSHO in a 39-bus system (PGC only)

Hr.	Discharge 1	Discharge 2	Discharge 3	Discharge 4	Thermal 1 /p.u.	Thermal 2 /p.u.	Thermal 3 /p.u.	Thermal 4 /p.u.	Thermal 5 /p.u.	Thermal 6 /p.u.	Wind 1 /p.u.	Wind 2 /p.u.	P_{total1}/p.u.	P_{total2}/p.u.
1	0.50	0.99	1.00	1.77	4.22	4.40	3.44	1.86	4.75	4.09	0.72	0.17	0.00	0.00
2	0.60	1.25	2.26	0.60	6.39	3.44	3.81	2.97	1.43	4.84	0.48	0.22	0.00	0.00
3	0.75	0.60	1.00	0.60	4.79	4.10	2.23	3.36	1.48	5.22	0.57	0.30	0.00	0.00
4	0.90	1.21	1.00	0.60	3.22	0.90	4.40	2.46	0.75	3.55	0.60	0.58	0.00	0.00
5	1.09	0.74	1.55	1.25	4.01	5.69	4.61	3.76	2.75	1.89	0.27	0.45	0.02	0.01
6	0.50	1.19	2.39	0.60	6.59	4.20	2.83	3.93	3.34	0.84	0.86	0.14	0.24	0.25
7	1.33	0.60	1.00	0.60	3.33	6.44	1.58	5.54	3.48	3.34	0.11	0.31	0.54	0.58
8	0.90	1.29	1.00	1.76	4.76	5.92	2.84	4.98	1.67	3.90	0.13	0.39	1.46	1.35
9	0.79	0.60	1.60	1.45	4.17	4.64	0.93	6.47	4.46	3.41	0.38	0.43	1.20	1.40
10	0.94	0.60	1.00	1.05	3.83	5.62	1.80	3.46	4.63	3.57	0.37	0.54	1.58	1.95
11	0.50	0.60	1.60	0.60	2.92	2.15	3.98	4.02	4.04	4.11	0.34	0.56	2.50	3.12
12	0.57	0.98	2.03	1.97	6.41	4.89	4.47	0.87	1.84	4.08	0.54	0.14	2.57	2.86
13	1.03	0.60	2.21	0.60	5.73	4.10	6.10	2.85	3.39	3.14	0.54	0.56	2.46	3.17
14	0.50	0.60	1.00	1.84	9.25	5.81	1.68	1.21	2.84	4.03	0.80	0.35	1.12	1.46
15	0.63	0.80	1.00	0.60	5.82	6.03	3.81	3.72	4.03	3.47	0.41	0.55	1.30	1.50
16	0.87	0.72	2.91	0.60	2.66	2.36	3.87	5.99	3.03	5.47	0.06	0.49	1.30	1.94
17	0.98	0.60	2.42	1.77	7.23	1.29	5.68	3.96	2.06	4.71	0.20	0.45	0.87	0.99
18	0.65	0.76	1.16	1.48	9.67	6.01	2.87	4.21	4.16	5.77	0.80	0.24	0.60	0.40
19	0.88	0.60	1.00	1.75	9.81	4.65	6.69	6.21	4.94	5.03	0.89	0.30	0.10	0.08
20	0.62	0.63	1.00	1.02	10.36	5.82	4.37	5.07	4.58	4.94	0.33	0.53	0.00	0.00
21	0.51	0.61	2.36	2.00	8.18	6.48	6.16	5.74	1.84	4.01	0.55	0.51	0.00	0.00
22	0.50	0.75	1.00	0.60	5.74	5.40	4.18	3.03	3.92	4.18	0.75	0.25	0.00	0.00
23	1.47	1.42	2.94	1.99	4.86	4.26	1.74	3.57	3.59	3.26	0.50	0.58	0.00	0.00
24	1.47	1.47	2.93	1.72	4.97	4.20	3.64	4.97	2.12	2.34	0.81	0.24	0.00	0.00

Tab. 12 Optimization of CSHO for 39-bus system using just discharge and active power generation (ATC only)

Hr.	Discharge1	Discharge2	Discharge3	Discharge4	Thermal 1 /p.u.	Thermal 2/p.u.	Thermal 3/p.u.	Thermal 4/p.u.	Thermal 5/p.u.	Thermal 6/p.u.	Wind 1/ p.u.	Wind 2/ p.u.	P_{total1} / p.u.	P_{total2} / p.u.
1	0.50	0.60	1.00	0.85	8.82	1.75	4.88	5.18	2.05	1.03	0.45	0.43	0.00	0.00
2	0.85	0.60	1.00	1.80	8.13	3.32	0.76	2.96	3.64	2.87	0.21	0.53	0.00	0.00
3	0.65	1.23	2.91	0.60	3.14	4.96	2.02	5.18	1.35	4.41	0.59	0.51	0.00	0.00
4	0.50	0.60	1.00	0.60	5.04	2.61	2.25	1.39	1.92	3.12	0.84	0.33	0.00	0.00
5	1.09	0.60	1.00	1.91	1.54	6.26	4.03	5.60	3.52	1.77	0.84	0.02	0.01	0.01
6	0.51	0.89	2.33	0.60	7.48	2.96	2.77	3.36	3.55	2.73	0.31	0.11	0.23	0.21
7	0.50	1.25	1.13	0.60	5.55	5.34	5.28	2.06	3.72	1.90	0.33	0.45	0.65	0.39
8	0.52	0.76	2.81	1.61	9.50	3.17	0.87	4.35	4.21	2.97	0.63	0.21	1.31	1.61
9	0.50	0.70	1.00	1.84	7.03	5.80	5.23	1.34	3.61	2.18	0.45	0.03	0.91	1.02
10	0.50	0.60	1.34	0.60	1.74	5.83	7.07	2.98	3.70	4.08	0.21	0.45	1.30	1.01
11	1.15	0.93	1.19	0.60	7.23	3.94	0.69	2.09	0.95	5.38	0.44	0.16	2.61	3.13
12	0.50	0.60	1.00	1.76	2.91	6.37	1.55	4.91	2.95	3.91	0.51	0.53	2.46	2.45
13	0.50	0.93	1.00	1.86	3.77	6.41	3.28	3.03	4.96	4.42	0.14	0.35	2.46	2.59
14	1.12	0.60	1.39	1.80	7.58	6.02	0.66	5.44	3.48	1.83	0.47	0.02	0.96	1.70
15	0.50	1.45	2.55	0.60	10.01	5.27	4.39	1.93	3.14	2.66	0.72	0.54	1.29	1.42
16	0.94	0.69	1.00	1.99	8.81	0.87	4.94	0.57	3.08	3.31	0.75	0.21	1.57	1.52
17	0.50	0.60	1.00	0.60	6.73	1.68	5.52	5.85	4.41	2.36	0.66	0.30	0.95	0.80
18	0.88	0.60	2.25	0.77	9.55	6.20	5.78	1.29	4.90	6.22	0.39	0.58	0.53	0.34
19	1.20	1.13	1.19	1.44	8.38	5.81	6.40	6.33	4.08	6.38	0.53	0.42	0.09	0.09
20	1.09	0.60	2.10	1.07	9.97	5.45	6.51	3.39	5.04	5.26	0.19	0.28	0.00	0.00
21	0.87	0.60	1.67	0.60	7.51	4.77	6.97	3.93	3.74	6.08	0.76	0.24	0.00	0.00
22	1.15	0.66	1.58	1.64	9.15	4.01	5.47	4.29	1.44	1.94	0.13	0.15	0.00	0.00
23	1.49	1.49	2.92	1.83	2.63	5.74	6.03	5.79	0.80	0.94	0.61	0.24	0.00	0.00
24	1.50	1.50	2.94	1.28	6.65	5.25	3.63	2.71	3.51	1.60	0.12	0.24	0.00	0.00

Tab. 13 The 39-bus system's CSHO is multi-objective optimised for discharge and active power production

Hr.	Discharge1	Discharge2	Discharge3	Discharge4	Thermal 1 /p.u.	Thermal 2 /p.u.	Thermal 3 /p.u.	Thermal 4 /p.u.	Thermal 5 /p.u.	Thermal 6 /p.u.	Wind 1 / p.u.	Wind 2 / p.u.	P_{total1} / p.u.	P_{total2} / p.u.
1	1.12	0.60	1.15	1.40	5.39	3.50	0.80	3.65	4.04	4.95	0.55	0.59	0.00	0.00
2	0.50	0.90	2.04	0.60	3.50	5.92	1.97	3.36	4.86	3.82	0.02	0.44	0.00	0.00
3	1.21	0.60	1.30	0.60	6.25	4.29	1.66	5.61	1.30	1.55	0.76	0.50	0.00	0.00
4	1.42	0.94	1.51	0.60	4.62	2.48	1.44	3.52	3.16	1.32	0.06	0.19	0.00	0.00
5	0.50	0.70	1.80	0.60	8.11	3.11	2.23	3.91	4.09	2.75	0.35	0.06	0.01	0.01
6	0.68	0.91	1.56	0.60	4.10	3.49	4.99	2.11	5.01	2.30	0.16	0.04	0.30	0.26
7	0.50	0.96	1.28	0.60	6.35	3.82	4.09	2.04	0.78	6.66	0.56	0.14	0.61	0.44
8	0.50	1.15	1.36	0.60	10.27	1.95	3.97	4.60	3.89	0.99	0.35	0.50	1.49	0.70
9	0.50	0.66	2.11	0.60	7.47	5.43	1.84	4.77	2.05	3.85	0.49	0.37	1.07	1.27
10	0.50	0.60	1.00	1.30	3.40	4.35	4.47	1.80	4.87	4.26	0.58	0.12	1.66	1.49
11	0.68	0.82	1.00	0.60	3.39	3.01	4.72	3.32	4.04	3.04	0.39	0.45	1.68	2.87
12	0.91	0.62	1.54	1.45	8.53	1.65	5.38	1.53	4.76	1.54	0.64	0.43	1.90	2.06
13	0.75	0.91	1.00	1.36	7.83	3.48	6.86	2.70	2.59	3.72	0.02	0.43	1.64	2.07
14	0.50	0.71	1.00	1.93	5.78	3.40	3.25	3.93	2.21	4.68	0.68	0.11	1.66	2.13
15	0.63	0.60	1.00	1.95	6.68	4.23	5.18	4.62	3.37	1.77	0.27	0.55	1.30	1.59
16	0.88	1.12	1.00	1.07	3.19	5.22	6.09	1.48	1.06	3.72	0.56	0.49	1.67	2.11
17	0.98	0.66	2.83	1.92	6.21	4.76	0.57	5.85	2.25	5.42	0.53	0.34	0.67	0.63
18	0.71	0.85	2.36	1.24	9.85	2.20	5.84	6.47	4.26	4.97	0.17	0.35	0.51	0.47
19	1.06	0.85	1.00	1.56	9.31	5.96	7.17	6.40	4.57	4.28	0.68	0.04	0.10	0.11
20	0.65	0.60	2.41	1.33	10.15	5.86	4.40	4.63	4.74	5.56	0.75	0.38	0.00	0.00
21	0.64	0.60	1.00	1.90	9.63	5.96	6.56	3.92	2.99	3.67	0.53	0.05	0.00	0.00
22	0.75	0.85	2.22	1.71	8.37	0.69	6.00	4.54	4.52	1.82	0.25	0.26	0.00	0.00
23	1.43	1.50	2.79	1.80	0.76	6.13	5.56	5.48	1.79	2.52	0.31	0.32	0.00	0.00
24	1.49	1.49	2.90	1.61	8.82	3.17	2.23	1.08	2.64	4.80	0.58	0.21	0.00	0.00

Tab. 14 Status of CSHO Case A, B, and C solar panels' ON/OFF switches in the IEEE 39-bus system

Hr.	Study: Case A		Study: Case B		Study: Case C	
	Solar $unit_1$	Solar $unit_2$	Solar $unit_1$	Solar $unit_2$	Solar $unit_1$	Solar $unit_2$
1	0000000000000	0000000000000	0000000000000	0000000000000	0000000000000	0000000000000
2	0000000000000	0000000000000	0000000000000	0000000000000	0000000000000	0000000000000
3	0000000000000	0000000000000	0000000000000	0000000000000	0000000000000	0000000000000
4	0000000000000	0000000000000	0000000000000	0000000000000	0000000000000	0000000000000
5	1010100011111	1001000101000	0100101111110	0011010110001	0110110111011	0101110111000
6	0100110100111	0111110101110	0001111111100	1011100110000	0110111110110	0011110010111
7	1000101000110	1111000011001	1111100101001	1111000000001	0010110011001	0001001101001
8	1101101110011	0000011111101	1011001001111	0001111110101	0101111110100	0101100000101
9	0010011100111	1111001110111	0001011100000	0100000101100	0011011000110	0011101001111
10	1101000010101	0010011101011	0110101000001	1000100010000	0110101001100	1101101000011
11	1110111010011	1110110111101	1100000110011	1101110010111	0101011100000	0111011101011
12	1101011010101	1100111000111	0000011100110	0101101101000	0101000000001	1000101010011
13	1010100110011	1011101111101	1011100001110	1111101011100	1001110100000	0011011100001
14	1010000110000	1100000110001	0010000011000	0010000101001	1111110000001	1100110110111
15	0001010100110	0100010111001	0100010110010	0100110010010	0111101010000	1000011011011
16	1010010101100	1111101111011	1001010111100	0001111111101	1100001101110	0110111110111
17	1101001010011	1101110100110	1001010101110	0100010110110	0011001100100	1000100011100
18	1000111111110	1010000100101	0110110011011	0011101100000	1101110001011	1111101100010
19	0111010011110	0101101101000	0011011101100	0110011010110	1010110111110	1001100110111
20	0000000000000	0000000000000	0000000000000	0000000000000	0000000000000	0000000000000
21	0000000000000	0000000000000	0000000000000	0000000000000	0000000000000	0000000000000
22	0000000000000	0000000000000	0000000000000	0000000000000	0000000000000	0000000000000
23	0000000000000	0000000000000	0000000000000	0000000000000	0000000000000	0000000000000
24	0000000000000	0000000000000	0000000000000	0000000000000	0000000000000	0000000000000

Finally, the authors discussed multi-objective optimization by focusing on lowering the total cost while increasing the ATC, as shown in Case C. Compared to the other algorithms, the CSHO approach yielded the best results, with a value of $447.509/24 h. This was performed while considering 30 separate trial runs, and the values for all control parameters are shown in Tabs. 11-13 for respective best run. Fig. 5 shows a three-dimensional picture of how the voltage changes over 24 h in each of the three scenarios.

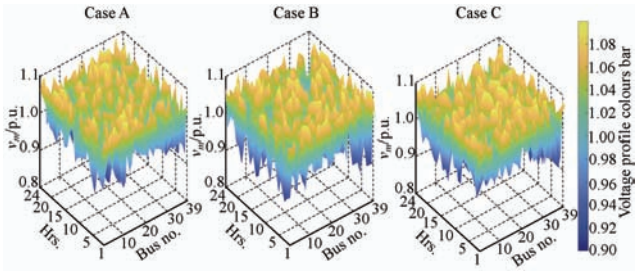

Fig. 5 Voltage across a 39-bus system subjected to a variety of stress conditions (Bus voltage of IEEE 39 bus: 24 h)

4.3 Research and findings of NRPG 246-bus test system

In addition, research is being conducted on the NRPG 246-bus test system. All information was gathered from published research [52, 55]. According to previous reports, bus 40 was used as the source, bus 200 was used as the sink, and the ATC discovered in Ref. [52] is 3.228 2 p.u.. BBO, GWO, and SHO were compared to determine the effectiveness of the CSHO. As indicated in Tab. 15, applying CSHO results in an ATC of 3.291 6 p.u., which is significantly better than the results obtained by BBO (3.255 2 p.u.), GWO (3.276 5 p.u.), and SHO (3.280 8 p.u.) without violating any power system constraints. This is the case even though none of the other methods caused violations.

Tab. 15 NRPG 246-bus results for Case B

Parameters	Case B OPF [52]	BBO	GWO	SHO	CSHO
Bestfit-val	NA	0.307	0.305	0.304	0.303
ATC/p.u.	3.228	3.255	3.276	3.280	3.291
CPU time/s	NA	426	450	521	1 889
Voltage mismatch	NA	0	0	0	0
Line flow violation (if any)	Yes (199-200)	0	0	0	0

5 Conclusions

In this study, we discuss a new strategy for ATC computation and power cost optimization that uses hydro, solar, and wind power. The proposed method, called the CSHO method, has been investigated and shown to be more efficient than previous metaheuristic optimizations in terms of the number of iterations and cost values. It also exhibits better convergence properties. It is necessary to consider both the unpredictability of wind power and load requirements. Another purpose of this study is to include solar, wind, and hydro units in typical thermal-producing units to decrease the total cost of active power production. The following is an outline of the outcomes produced by the proposed methodology. Similar heuristic approaches, such as SCA, BBO, GWO, and SHO, all produced similar results, which were shown in the most recent study. Utilizing the IEEE 9-bus is one way to demonstrate the effectiveness of the proposed solution. Test systems for the IEEE 39-bus and NRPG 246-bus, including three separate use cases were examined. In every case, both the convergence characteristics and efficiency of computing of the new method are much better than those of the old methods. This article discusses the difficulties of ATC and RES-thermal scheduling for 24 h, which adds to the overall uniqueness of the study.

References

[1] G C Ejebe, J Tong, J G Waight, et al. Available transfer capability calculations. *IEEE Transactions on Power Systems*, 1998, 13(4): 1521-1527.

[2] The World Bank. Electric power consumption (kW • h per capita). [2020-11-03]. https://data.worldbank.org/indicator/EG.USE.ELEC.KH.PC.

[3] Government of India, Central Electricity Authority, Ministry of Power. Growth of electricity sector in India from 1947-2020. [2021-06-09]. https://cea.nic.in/wp-content/uploads/pdm/2020/12/growth_2020.pdf.

[4] A R Bergen, V Vittal. Power systems analysis. 2nd ed. Chennai: Pearson Education, 2009.

[5] H D Chiang, H Li. On-line ATC evaluation for large-scale power systems: Framework and tool. Applied mathematics for restructured electric power systems: optimization, control, and computational intelligence.

Heidelberg: Springer, 2005.

[6] N Kumar, B K Panigrahi, B Singh. A solution to the ramp rate and prohibited operating zone constrained unit commitment by GHS-JGT evolutionary algorithm. *International Journal of Electrical Power & Energy Systems*, 2016, 81: 193-203.

[7] A G Bakirtzis, P N Biskas. A decentralized solution to the DC-OPF of interconnected power systems. *IEEE Transactions on Power Systems*, 2003, 18(3): 1007-1013.

[8] Q Morante, N Ranaldo, A Vaccaro, et al. Pervasive grid for large-scale power systems contingency analysis. *IEEE Transactions on Industrial Informatics*, 2006, 2(3): 165-175.

[9] J H Liu, C C Chu. Iterative distributed algorithms for real-time available transfer capability assessment of multiarea power systems. *IEEE Transactions on Smart Grid*, 2015, 6(5): 2569-2578.

[10] L Xie, Y Chen, H Liao. Distributed online monitoring of quasi-static voltage collapse in multi-area power systems. *IEEE Transactions on Power Systems*, 2012, 27(4): 2271-2279.

[11] R Ebrahimian, R Baldick. State estimation distributed processing for power systems. *IEEE Transactions on Power Systems*, 2000, 15(4): 1240-1246.

[12] D M Falcao, F F Wu, L Murphy. Parallel and distributed state estimation. *IEEE Transactions on Power Systems*, 1995, 10(2): 724-730.

[13] P Šulc, S Backhaus, M Chertkov. Optimal distributed control of reactive power via the alternating direction method of multipliers. *IEEE Transactions on Energy Conversion*, 2014, 29(4): 968-977.

[14] Q Yang, J A Barria, T C Green. Communication infrastructures for distributed control of power distribution networks. *IEEE Transactions on Industrial Informatics*, 2011, 7(2): 316-327.

[15] L Wang, Q Li, B Zhang, et al. Robust multi-objective optimization for energy production scheduling in microgrids. *Engineering Optimization*, 2019, 51(2): 332-351.

[16] X Li, K Deb, Y Fang. A derived heuristics based multi-objective optimization procedure for micro-grid scheduling. *Engineering Optimization*, 2017, 49(6): 1078-1096.

[17] L Pan, W Xu, L Li, et al. Adaptive simulated binary crossover for rotated multi-objective optimization. *Swarm and Evolutionary Computation*, 2020: 100759.

[18] T Rasku, J Miettinen, E Rinne, et al. Impact of 15-day energy forecasts on the hydro-thermal scheduling of a future nordic power system. *Energy*, 2020, 192: 116668.

[19] Z Ma, S Wang, S Li, et al. Long-term coordination for hydro-thermal-wind-solar hybrid energy system of provincial power grid. *Energy Procedia*, 2019, 158: 6231-6235.

[20] M R Ebrahimi, N Amjady. Adaptive robust optimization framework for day-ahead microgrid scheduling. *International Journal of Electrical Power & Energy Systems*, 2019, 107: 213-223.

[21] M Eslahi, A F Nematollahi, B Vahidi. Day-ahead scheduling of centralized energy storage system by proposed stochastic minlp-based bi-objective optimization approach. *Electric Power Components and Systems*, 2020: 1-24.

[22] C Elberg, S Hagspiel. Spatial dependencies of wind power and interrelations with spot price dynamics. *European Journal of Operational Research*, 2015, 241(1): 260-272.

[23] H M Dubey, M Pandit, B K Panigrahi. An overview and comparative analysis of recent bio-inspired optimization techniques for wind integrated multi-objective power dispatch. *Swarm and Evolutionary Computation*, 2018, 38: 12-34.

[24] S Zhao, Y Fang, Z Wei. Stochastic optimal dispatch of integrating concentrating solar power plants with wind farms. *International Journal of Electrical Power & Energy Systems*, 2019, 109: 575-583.

[25] Y Wu, K Chen, H Xu, et al. An innovative method for offshore wind farm site selection based on the interval number with probability distribution. *Engineering Optimization*, 2017, 49(12): 2174-2192.

[26] H Yang, L Zhang, K Meng, et al. Optimal scheduling of hydro-thermal power systems considering the flood risk of cascade reservoirs. *Engineering Optimization*, 2017, 49(8): 1299-1316.

[27] V Sharma, R Jha, R Naresh. An augmented lagrange programming optimization neural network for short-term hydroelectric generation scheduling. *Engineering Optimization*, 2005, 37(5): 479-497.

[28] A K Barisal, N C Sahu, R C Prusty, et al. Short-term hydrothermal scheduling using gravitational search algorithm. *2012 2nd International Conference on Power, Control and Embedded Systems*, 2012: 1-6.

[29] M Eslahi, A F Nematollahi, B Vahidi. Day-ahead scheduling of centralized energy storage system by proposed stochastic minlp-based bi-objective optimization approach. *Electric Power Components and Systems*, 2020: 1-24.

[30] G L Decker, A D Brooks. Valve point loading of turbines. *Transactions of the American Institute of Electrical Engineers. Part III: Power Apparatus and Systems*, 1958, 77(3): 481-484.

[31] M I Alomoush. Application of the stochastic fractal search algorithm and compromise programming to combined heat and power economic-emission dispatch. *Engineering Optimization*, 2019: 1-19.

[32] J Xu, F Wang, C Lv, et al. Carbon emission reduction and reliable power supply equilibrium based daily scheduling towards hydro-thermal-wind generation system: A perspective from China. *Energy Conversion and Management*, 2018, 164: 1-14.

[33] R S Patwal, N Narang. Optimal generation scheduling of pumped storage hydro-thermal system with wind energy sources. *Applied Soft Computing*, 2020: 106345.

[34] N Hakimuddin, I Nasiruddin, T S Bhatti, et al. Optimal automatic generation control with hydro, thermal, gas, and wind power plants in 2-area interconnected power system. *Electric Power Components and Systems*, 2020, 48(6-7): 558-571.

[35] G Shaghaghi-shahr, M Sedighizadeh, M Aghamohammadi, et al. Optimal generation scheduling in microgrids using mixed-integer second-order cone programming. *Engineering Optimization*, 2020: 1-29.

[36] F Zhu, P Zhong, B Xu, et al. Short-term stochastic optimization of a hydro-wind-photovoltaic hybrid system under multiple uncertainties. *Energy Conversion and Management*, 2020, 214: 112902.

[37] M Basu. Economic environmental dispatch of solar-wind-hydro-thermal power system. *Renewable Energy Focus*, 2019, 30: 107-122.

[38] K Jamuna, K S Swarup. Biogeography based optimization for optimal meter placement for security constrained state estimation. *Swarm and Evolutionary Computation*, 2011, 1(2): 89-96.

[39] Y Chen, F He, H Li, et al. A full migration bbo algorithm with enhanced population quality bounds for multimodal biomedical image registration. *Applied Soft Computing*, 2020: 106335.

[40] P K Roy, S P Ghoshal, S S Thakur. Optimal Var control for improvements in voltage profiles and for real power loss minimization using biogeography based optimization. *International Journal of Electrical Power & Energy Systems*, 2012, 43(1): 830-838.

[41] S Mirjalili, S M Mirjalili, A Lewis. Grey wolf optimizer. *Advances in Engineering Software*, 2014, 69: 46-61.

[42] K Majumdar, P Das, P K Roy, et al. Solving OPF problems using biogeography based and grey wolf optimization techniques. *International Journal of Energy Optimization and Engineering (IJEOE)*, 2017, 6(3): 55-77.

[43] H M Goodarzi, M H Kazemi. An optimal autonomous microgrid cluster based on distributed generation droop parameter optimization and renewable energy sources using an improved grey wolf optimizer. *Engineering Optimization*, 2018, 50(5): 819-839.

[44] Z Miao, X Yuan, F Zhou, et al. Grey wolf optimizer with an enhanced hierarchy and its application to the wireless sensor network coverage optimization problem. *Applied Soft Computing*, 2020: 106602.

[45] S Gupta, K Deep. A novel random walk grey wolf optimizer. *Swarm and Evolutionary Computation*, 2019, 44: 101-112.

[46] F Fausto, E Cuevas, A Valdivia, et al. A global optimization algorithm inspired in the behavior of selfish herds. *Biosystems*, 2017, 160: 39-55.

[47] M Cornick, B Hunt, E Ott, et al. State and parameter estimation of spatiotemporally chaotic systems illustrated by an application to Rayleigh-Bénard convection. *Chaos*, 2009, 19(1): 013108.

[48] K U Shahna, A Mohamed. A novel image encryption scheme using both pixel level and bit level permutation with chaotic map. *Applied Soft Computing*, 2020, 90: 106162.

[49] S A G Kaur. Chaotic whale optimization algorithm. *Journal of Computational Design and Engineering*, 2018, 5: 275-284.

[50] K Dasgupta, P K Roy, V Mukherjee. Power flow based hydro-thermal-wind scheduling of hybrid power system using sine cosine algorithm. *Electric Power Systems Research*, 2020, 178: 106018.

[51] Grainger College of Engineering. Illinois Center for a Smarter Electric Grid (ICSEG). Available at for IEEE 39. [2019-11-03]. https://icseg.iti.illinois. edu/ieee-39-bus-system-2/.

[52] R H Bhesdadiya, R M Patel. Available transfer capability calculation using deterministic methods: A case study of

Indian power system. *2016 International Conference on Electrical*, *Electronics*, *and Optimization Techniques (ICEEOT)*, IEEE, 2016: 2261-2264.

[53] Grainger College of Engineering. Illinois Center for a Smarter Electric Grid (ICSEG). Available at for IEEE 9. [2019-12-03]. https://icseg.iti.illinois.edu/wscc-9-bus-system/.

[54] M A Pai. Future research issues. In energy function analysis for power system stability. Heidelberg: Springer, 1989.

[55] IIT Kanpur. Facilities of research-lab power system. Available at for NRPG 246. [2019-11-03]. https://www.iitk.ac.in/eeold/facilities/Research_labs/Power_System/NRPG-DATA.pdf.

Kingsuk Majumdar received his Ph.D. degree and M.Tech. in Electrical Engineering from NIT Durgapur, 2023 and 2013, respectively. He is an Assistant Professor in the Department of Electrical Engineering, Dr. B C Roy Engineering College, Durgapur. His research interests include optimization, power system, power electronics, etc. He has guided several B.Tech. and three M.Tech. students. He is an associate member of The Institution of Engineers (India).

Provas Kumar Roy obtained Ph.D. degree in Electrical Engineering from National Institute of Technology Durgapur in 2011. He received his Master degree in Electrical Machine in 2001 from Jadavpur University. He finished his Engineering studies in Electrical Engineering from Regional Engineering College (Presently Known as National Institute of Technology) Durgapur. Presently, he is working as a Professor in Electrical Engineering Department at Kalyani Government Engineering College, West Bengal, India. He was the recipient of the Outstanding Reviewer Award for IJEPES (Elsevier, 2018), EAAI (Elsevier, 2017), Renewable Energy Focus (Elsevier, 2018), ASEJ (Elsevier, 2017). He has published more than 150 research papers in national/international journals and conference and more than 75 journals published in reputed SCI and Scopus indexed Journals, and more than 10 book chapters and two books of international standard. Six research scholars have obtained their Ph.D. degree under his guidance and 8 students are perusing their Ph.D. under his guidance. His research interests include economic load dispatch, optimal power flow, FACTS, automatic generation control, radial distribution network, power system stabilizer, image processing, machine learning, evolutionary techniques, etc.

Subrata Banerjee (M'04-SM'15) has received his Ph.D. degree from IIT Kharagpur, India in 2005. He is working as Professor with the Department of Electrical Engineering, NIT, Durgapur, India. His research interests include modeling & control of switch-mode converters and inverters, multilevel inverters & different modulation techniques, electromagnetic levitation & control system design, etc. He has successfully completed few research and consultancy projects. He has authored about 195 research papers in national/international journals and conference records & 7 book chapters. He has guided 10 Ph.D. and 22 M.Tech. students and many are pursuing their degree under his guidance. He has filed three Indian patents out of which one has been granted. Prof. Banerjee is the recipient of several academic awards, including 10 nos. Best Paper Awards and TATA RAO Prize etc. He is a Fellow of the IE (India), the IETE (India), and the IET (UK), Senior Member IEEE (USA). He is serving as Associate Editor in IEEE Access (USA), IET Power Electronics (UK), IEEE TEC eNewsletter (USA), Transportation Electrification IEEE (USA).